AGU PUBLICATIONS

Geophysical Research Letters

RESEARCH LETTER
10.1002/2015GL063322

Key Points:
- Climate responses to orbital changes simulated with an Earth system model
- Model produces a larger ice-volume response to obliquity than precession
- Model results agree with early Pleistocene oxygen isotope records

Supporting Information:
- Text S1, Equation (S1), Figures S1–S4, and Table S1

Correspondence to:
C. R. Tabor,
crtabor@umich.edu

Citation:
Tabor, C. R., C. J. Poulsen, and D. Pollard (2015), How obliquity cycles powered early Pleistocene global ice-volume variability, *Geophys. Res. Lett.*, *42*, 1871–1879,doi:10.1002/2015GL063322.

Received 29 JAN 2015
Accepted 24 FEB 2015
Accepted article online 26 FEB 2015
Published online 19 MAR 2015

How obliquity cycles powered early Pleistocene global ice-volume variability

Clay R. Tabor[1], Christopher J. Poulsen[1], and David Pollard[2]

[1]Department of Earth and Environmental Sciences, University of Michigan, Ann Arbor, Michigan, USA, [2]Earth and Environmental Systems Institute, Pennsylvania State University, University Park, Pennsylvania, USA

Abstract Milankovitch theory proposes that the magnitude of high-latitude summer insolation dictates the continental ice-volume response by controlling summer snow melt, thus anticipating a substantial ice-volume contribution from the strong summer insolation signal of precession. Yet almost all of the early Pleistocene $\delta^{18}O$ records' signal strength resides at the frequency of obliquity. Here we explore this discrepancy using a climate-vegetation-ice sheet model to simulate climate-ice sheet response to transient orbits of varying obliquity and precession. Spectral analysis of our results shows that despite contributing significantly less to the summer insolation signal, almost 60% of the ice-volume power exists at the frequency of obliquity due to a combination of albedo feedbacks, seasonal offsets, and orbital cycle duration differences. Including eccentricity modulation of the precession ice-volume component and assuming a small Antarctic ice response to orbital forcing produce a signal that agrees with the $\delta^{18}O$ ice-volume proxy records.

1. Introduction

The most widely held theory for the relationship between ice-volume and insolation comes from the calculations of Milankovitch [*Milankovitch*, 1941], who proposed that high-latitude (HL) caloric summer half-year insolation determines the amount of snow cover that can survive summer melt and consequently, the amount of ice sheet growth or retreat. Changes in both Earth's obliquity and precession contribute significantly to the caloric summer half-year insolation forcing. Therefore, Milankovitch theory predicts that precession should produce a considerable ice-volume signal, a prediction borne out by climate models [e.g., *Berger et al.*, 1999]. However, the $\delta^{18}O$ ice-volume proxy records do not show the same signal. Rather, little spectral power exists at the frequency of precession, with practically none of the signal strength in the early Pleistocene (EP) (2.588–0.781 Ma) (Figure 1a) [*Lisiecki and Raymo*, 2007]. The surprising dominance of the obliquity signal in opposition to Milankovitch theory has been coined the "41 kyr problem" [*Raymo and Nisancioglu*, 2003]. Multiple hypotheses have been proposed to remedy the discrepancies between traditional Milankovitch theory and the ice-volume proxy record [e.g., *Clark and Pollard*, 1998; *Berger et al.*, 1999; *Philander and Fedorov*, 2003; *Raymo and Nisancioglu*, 2003; *Loutre et al.*, 2004; *Ravelo et al.*, 2004; *Vettoretti and Peltier*, 2004; *Huybers and Wunsch*, 2005; *Lee and Poulsen*, 2005; *Huybers*, 2006; *Raymo et al.*, 2006; *Lee and Poulsen*, 2008; *Tabor et al.*, 2014], but the contributions of these hypotheses to the ice-volume record have not been systematically explored with a model that includes both dynamic atmosphere and ice components.

Here we use an Earth system model to investigate the role of orbital forcing on climate. In contrast to previous studies, which model the climate responses to orbital forcing without dynamic land-ice [e.g., *Lee and Poulsen*, 2008; *Mantsis et al.*, 2011; *Erb et al.*, 2013] or with only individual orbital parameters [e.g., *Tabor et al.*, 2014], our simulations use a series of transient orbital configurations with dynamic land-ice and simultaneously varying obliquity and precession. This model setup allows us to explore the climate interactions produced by combined orbital forcings and use statistical time series analysis to make direct comparisons between the modeled ice-volume cycles and proxy data. We find that the ice-volume signal is not entirely a direct response to summer insolation. Instead, climate feedbacks involving sea ice, vegetation, and clouds, seasonal offset of the insolation forcing from precession and greater cycle duration of obliquity enhance the ice-volume response to obliquity relative to precession. Combined, these factors give obliquity about 60% of the ice-volume power. Though substantially muted, our experiments still produce a larger precession ice-volume response than recorded in Pleistocene $\delta^{18}O$ records. In our discussion, we provide methods to resolve the remaining discrepancies between the modeled ice-volume signal and the $\delta^{18}O$ records of the early Pleistocene. We quantitatively show that the ice-volume spectral power shifts to the obliquity cycle frequency when modulating the precession

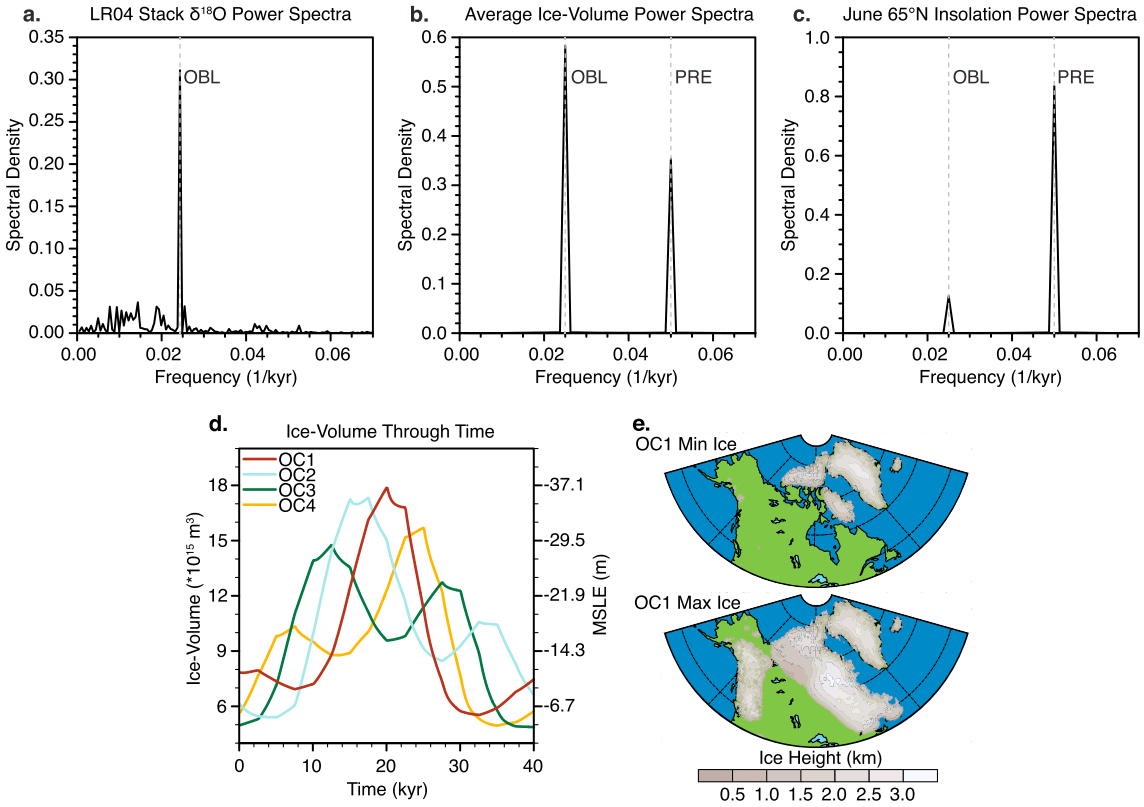

Figure 1. The 41 kyr problem and the ice sheet responses to orbital forcing. (a) The power spectra of EP (2.588–0.781 Ma) detrended δ^{18}O stack [*Lisiecki and Raymo*, 2005]. Almost all of the power is at the frequency of obliquity. (b) Average standardized spectral power distribution of the ice-volume response to our four transient orbital configurations (OC1–OC4). The ice-volume response produces more power at the frequency of obliquity than precession. (c) Plot of the 65°N June insolation spectral power distribution. Here we chose 65°N June insolation because it is a standard commonly associated with modeling studies of Milankovitch theory. Vertical dashed gray lines highlight the location of the obliquity and precession frequencies. (d) Simulated ice-volume (10^{15} m^3) for our four transient orbital configurations (OC1–OC4). (e) The minimum and maximum ice extents for OC1. Ice extents for OC2–OC4 are comparable.

component by eccentricity or including a small amount of ice-volume response from Antarctica. Our findings are an important step toward explaining the ice-volume records of the early Pleistocene.

2. Methods

2.1. Earth System Model

We use a global climate-vegetation-ice model consisting of the Global Environmental and Ecological Simulation of Interactive Systems (GENESIS) 3.0 general circulation model (GCM) [*Alder et al*., 2011], the Global biome model version 4 (BIOME4) vegetation model [*Kaplan et al*., 2003], and the Pennsylvania State University (PSU) ice sheet model [*Pollard and DeConto*, 2012]. The GENESIS 3.0 GCM contains coupled atmosphere (atmospheric general circulation model (AGCM)) and land surface (LSX) components. The AGCM is run at T31 horizontal resolution (~3.75°) with 18 vertical sigma levels, and the LSX model is run at 2° horizontal resolution with a 50 m slab ocean that calculates ocean heat transport through linear diffusion based on local temperature gradient and a latitude-dependent diffusion coefficient and dynamic sea ice. GENESIS 3.0 is synchronously coupled with the BIOME4 vegetation model. Ecosystem types are calculated annually from a combination of prescribed soil and atmospheric CO_2, and monthly mean GCM averages of temperature, insolation, and precipitation. The PSU ice sheet model is a 3-D thermomechanical model; here its marine ice capability is suppressed, so all dynamics are based on the shallow ice approximation. Further, we use an insolation/temperature melt scheme (ITM) [*Pollard*, 1980; *van den Berg et al*., 2008] in place of the commonly employed positive-degree-day (PDD) melt scheme. *Robinson et al*. [2010] find that the ITM scheme produces a heightened ice sheet sensitivity compared to the PDD scheme, which better represents ice-volume changes over long time scales.

2.2. Experiment Design

We force the Earth system model with a series of four idealized, transient orbital configurations that represent the extremes of the Pleistocene [*Berger and Loutre*, 1991] to explore the interactions of obliquity and precession on climate and Northern Hemisphere (NH) ice-volume. For ease and efficiency, obliquity and precession vary through time as pure (simple, idealized) sinusoids with durations of 40 kyr and 20 kyr respectfully, approximations of the actual durations. The four orbital configurations (OC1–OC4) differ only in the timing of precession with respect to obliquity. From a fixed obliquity perspective, precession cycles are staggered by 5 kyr (Table S1 in the supporting information). All experiments are initialized with modern continental configuration and land surface type including modern Greenland and Antarctica, and no other ice sheets. The dynamic ice sheet domain includes Greenland and North America above 40°N. Due to computational costs, we use an asynchronous coupling technique to capture the responses of the Earth system to the transient orbits [e.g., *Birchfield et al*., 1981; *Herrington and Poulsen*, 2012]. We look at the climate response to orbital forcing both with (climate ice) and without (climate only) a dynamic ice sheet. For experiments without dynamic ice, the ice sheet model is not run, and land surface type and topography are held fixed at modern. Because EP greenhouse gas (GHG) fluctuations are not well known, we use values representing the average of the last 400 kyr ($CO_2 = 230$ ppmv, $CH_4 = 520$ ppbv, and $N_2O = 250$ ppbv) [*Petit et al*., 1999; *Bender*, 2002]. See supporting information for additional experiment design details.

3. Results

3.1. Ice-Volume Spectral Power

The ice-volume responses to our four transient orbital configurations produce mean sea level equivalent (MSLE) variations between 25 and 31 m (Figure 1d). Transient orbital forcing causes substantial variations in the areal extent of both the Laurentian and Cordilleran ice sheets (Figure 1e). Spectral analysis of the transient ice-volume signals shows that, on average, there is more power at the frequency of obliquity ($40\,kyr^{-1}$) than precession ($20\,kyr^{-1}$) (Figure 1b). There is some minor variability in the power density distribution between the four transient orbital configurations, but the greatest signal strength is always at the frequency of obliquity (Figure S1). In contrast, most of the spectral power of June 65°N insolation intensity, a commonly used metric for Milankovitch forcing in climate models, is at the frequency of precession (Figure 1c), which indicates this common Milankovitch metric is not a direct driver of ice-volume in our model. Like other modeling studies, our results also display too great of an ice-volume response to precession, which is absent in the ice-volume proxy records of the EP [*Lisiecki and Raymo*, 2005; *Huybers*, 2007] (Figure 1a). We propose several explanations for this discrepancy below.

3.2. Climate Signal Decomposition

The prominent ice-volume response at the obliquity frequency occurs through climate amplification of the insolation forcing. To better and more easily understand the climate responses to changes in orbital forcing, we decompose the climate responses of the climate-only experiments into contributions from obliquity and precession using a least squares fitting procedure similar to that of *Jackson and Broccoli* [2003]. The deviation of a given variable through time from its mean, X(t), is expressed as follows:

$$\mathrm{X}(t) = A_o \phi'(t) + A_p \cos\left[\lambda(t) - \phi_p\right] + R(t) \quad (1)$$

where ϕ' is the deviation of obliquity from its mean, λ is the longitude of perihelion, and R is the residual that accounts for nonlinearity of the system. The fitting procedure finds the amplitude of response to obliquity A_o, the amplitude of response of precession A_p, and the phase angle of precession ϕ_p. Because eccentricity is constant, it is excluded from equation (1).

The following analysis focuses on the North American (NA) HL (area between 55 and 75°N and 57 and 165°W) responses of insolation, surface-absorbed shortwave radiation, and near-surface temperature because these variables are used to calculate ablation in the ice sheet model (equation (S1)). Precipitation also contributes to the mass balance of the ice sheets; however, our ice-volume responses are dominated by ablation, not accumulation, a finding mirrored in other studies [e.g., *DeConto et al*., 2008; *Tabor et al*., 2014]. Furthermore, precipitation responses to orbital changes are less linear than surface-absorbed shortwave radiation and near-surface temperature, which reduces the appropriateness of the least squares fitting procedure. Conversely, the NA HL surface-absorbed shortwave radiation and near-surface temperature responses to

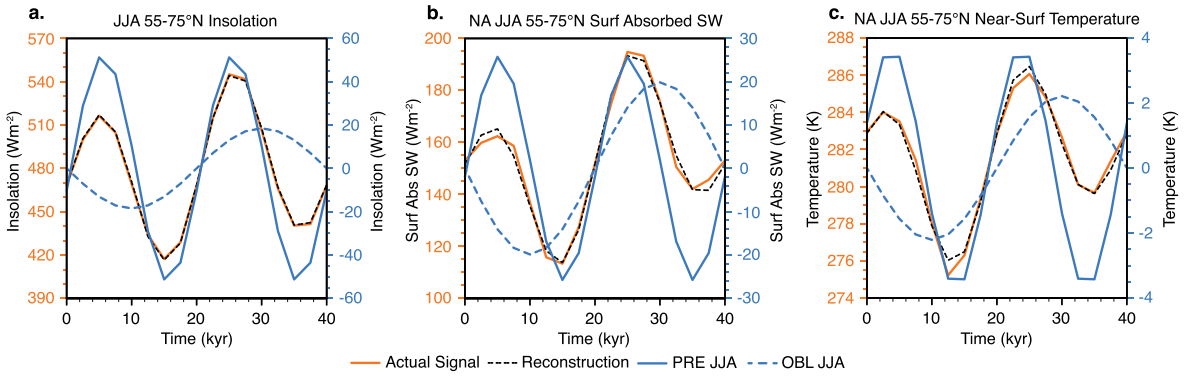

Figure 2. Decomposition of NA HL summer insolation, surface-absorbed shortwave radiation, and near-surface temperature into obliquity and precession components. Spatial and temporal averages of NA HL (55–75°N, 57–165°W) June, July, and August (JJA) signals from OC1 over an orbital cycle. The model responses (solid orange line) and least squares reconstructions (dashed black line) are plotted on the primary *y* axis. The contributions from obliquity (dashed blue line) and precession (solid blue line) are plotted on the secondary *y* axis. (a) The insolation forcing (W m^{-2}). (b) The amount of surface-absorbed shortwave radiation (W m^{-2}). (c) The near-surface temperature (K) response. Obliquity contributes nearly twice as much to the NA HL summer variations in surface-absorbed shortwave radiation and near-surface temperature as it does to insolation forcing, which suggests internal amplification.

insolation changes are quite linear in the summer months. The decomposed climate responses discussed below are spatially, temporally, and experiment-averaged signal decompositions from all four transient orbital configurations. We find that the climate responses are similar for all orbital configurations, and therefore, Figure 2 shows the outputs of OC1 for simplicity. Note, we focus on NA for our analysis because it is within the dynamic ice domain; however, similar responses are found throughout the NH HL.

3.2.1. Summer Season Feedbacks

The total HL June, July, and August (later referred to as summer) insolation variability is over 124 W m^{-2} (Figure 2a, orange line). By decomposing the summer insolation forcing into obliquity and precession components, we find that only 11% of the variance is due to obliquity with the remaining 89% attributable to precession. On the other hand, the variance of the 78 W m^{-2} fluctuations in NA HL summer surface-absorbed radiation is split 36% to 62%, and the 10°C fluctuations in NA HL summer near-surface temperature are split 24% and 75% between obliquity and precession, respectively (Figures 2b and 2c). While precession still controls the majority of the NA HL summer surface-absorbed shortwave radiation and near-surface temperature responses, obliquity contributes nearly twice what would be expected assuming a direct surface response to insolation forcing.

The amplification of the surface responses to insolation forcing is mainly a result of albedo feedbacks that are significantly larger for obliquity than the incoming insolation would suggest. For instance, obliquity forcing accounts for 49% of the NA HL summer planetary albedo variance. The planetary albedo signal is, in part, a result of variations in surface albedo, which oscillates by 0.14 during the summer months, with a 39% to 57% split in the variance between obliquity and precession, respectively. Changes in NH HL sea ice fractional coverage, split 57% to 38% between obliquity and precession, and NA HL tundra/boreal forest exchange, split 38% to 58% between obliquity and precession, cause much of the summer surface albedo variability. We focus on the summer response because of its significance to ice ablation, but the sea ice contribution from obliquity is even larger in the spring and fall months. Furthermore, in the model, vegetation distributions do not vary seasonally, enhancing the obliquity response all year. In addition to their direct effects, the surface albedo feedbacks of sea ice and vegetation also influence the amount of snow cover through melting and canopy masking, which further magnifies the surface albedo response. However, the snow cover fluctuations are less linear than sea ice and vegetation and, therefore, are difficult to decompose through least squares fitting. These surface albedo feedbacks allow the surface to warm disproportionately relative to the insolation forcing, amplifying the obliquity signal relative to precession.

The obliquity contribution to cloud albedo response is also larger than the insolation forcing with a 47% to 46% split in variance between obliquity and precession. The total cloud albedo changes over an orbital cycle are only 0.033 and are mainly a result of changes in stratus clouds. In these experiments cooler HL summer temperatures during periods of low summer insolation allow more snow and soil moisture to persist into the

summer months. The surface moisture source, combined with a weak low-level lapse rate due to the cold surface, allows greater low-level relative humidity and stratus cloud cover. In the summer, enhanced cloud cover reduces surface-absorbed shortwave radiation and temperature and provides a positive ice-volume feedback. As previously mentioned, the changes in cloud albedo are fairly small.

The amplified responses of sea ice fraction and vegetation to obliquity relative to precession are a consequence of the annual-mean insolation changes due to obliquity. Latitudinal redistribution of annual-mean insolation due to changes in obliquity causes variations in ocean-absorbed shortwave to be greater than those due to precession, resulting in more ocean heat release and a larger sea ice response. Likewise, obliquity forced annual-mean insolation variations in the high latitudes produce a larger range of annual temperature and sunlight reaching the surface than precession, which boosts the range of net-primary productivity and allows for a greater vegetation transition between tundra and boreal forest. Other studies have also found important vegetation and sea ice responses to orbital variations [e.g., *Gallimore and Kutzbach*, 1995, 1996; *Tuenter et al*., 2004, 2005; *Claussen et al*., 2006; *Horton et al*., 2010; *Tabor et al*., 2014]; however, this research is the first to examine surface feedbacks under the combined effects of obliquity and precession with a complex Earth system model that includes dynamic land-ice.

3.2.2. Precession Seasonal Insolation Offset

In addition to differences in summer insolation and climate response, obliquity and precession also contribute differently to insolation timing and duration. Even though precession dominates the summer insolation signal, precession produces no changes in annual-mean insolation. Conversely, obliquity does alter the latitudinal distribution of annual-mean insolation, especially in the HLs. The difference in mean-annual insolation between obliquity and precession works to amplify the climate influence of obliquity while dampening the influence of precession [*Huybers*, 2006]. Using the least squares signal decomposition, we illustrate the difference in insolation forcing from precession and obliquity by examining differences in NH HL insolation forcing between April and September (Figure S2a). When April insolation forcing from precession is anomalously large, September insolation forcing from precession is anomalously small, and vice versa. The difference in seasonal phasing of the precession insolation signal causes offset in the NA HL surface-absorbed shortwave (Figure S2b) and, to a lesser amount due to inertia of the system, near-surface temperature (Figure S2c) while the concurrent seasonal phasing of obliquity amplifies the response. These differences in seasonal forcing shorten the melt season for precession but lengthen it for obliquity.

The amount of ablation that occurs during the spring and fall is small, about 5% of the total climate-only HL NA land potential ablation (based on equation (S1)), which makes seasonal offset of secondary importance in our experiments. However, our experimental design uses relatively low-GHG concentrations. While not well constrained, the EP was potentially warmer than the mean climate produced by our model configuration. In a warmer world, the melt threshold is more easily reached, allowing a longer melt season that both enhances the seasonal cancelation effect from precession and melt of obliquity [*Huybers and Tziperman*, 2008]. Therefore, our experiments represent a conservative estimate of the seasonal offset response to precession forcing.

3.3. Cycle Frequencies and Nonequilibrium

Even with surface amplification of obliquity signal and seasonal offset of precession forcing, the ablation response favors precession; however, the ice-volume response favors obliquity. Much of this remaining discrepancy is a consequence of the nonequilibrium response of the ice sheets to orbital forcing in combination with differences in cycle duration between obliquity and precession [*Roe*, 2006; *Huybers and Tziperman*, 2008]. Our results show that ablation has a nearly linear control on ice-volume rate of change while ice-volume lags ablation and has no direct correlation (Figure S3). Using these relationships, we can describe the magnitude of the ice-volume as a combination of obliquity and precession [*Huybers and Tziperman*, 2008]:

$$V = \frac{A_o}{\omega_o}\sin(\omega_o t) + \frac{A_p}{\omega_p}\sin(\omega_p t) \tag{2}$$

where t is time, V is ice-volume, A_o is the amplitude response to obliquity, ω_o is the frequency of obliquity (40 kyr^{-1}), A_p is the amplitude response to precession, and ω_p is the frequency of precession (20 kyr^{-1}). Here we assume a 90° phase lag response of the ice sheets to forcing. Equation (2) demonstrates that the influence of obliquity on the ice-volume rate of change is relatively enhanced simply because the frequency of the obliquity cycle is half that of the precession cycle.

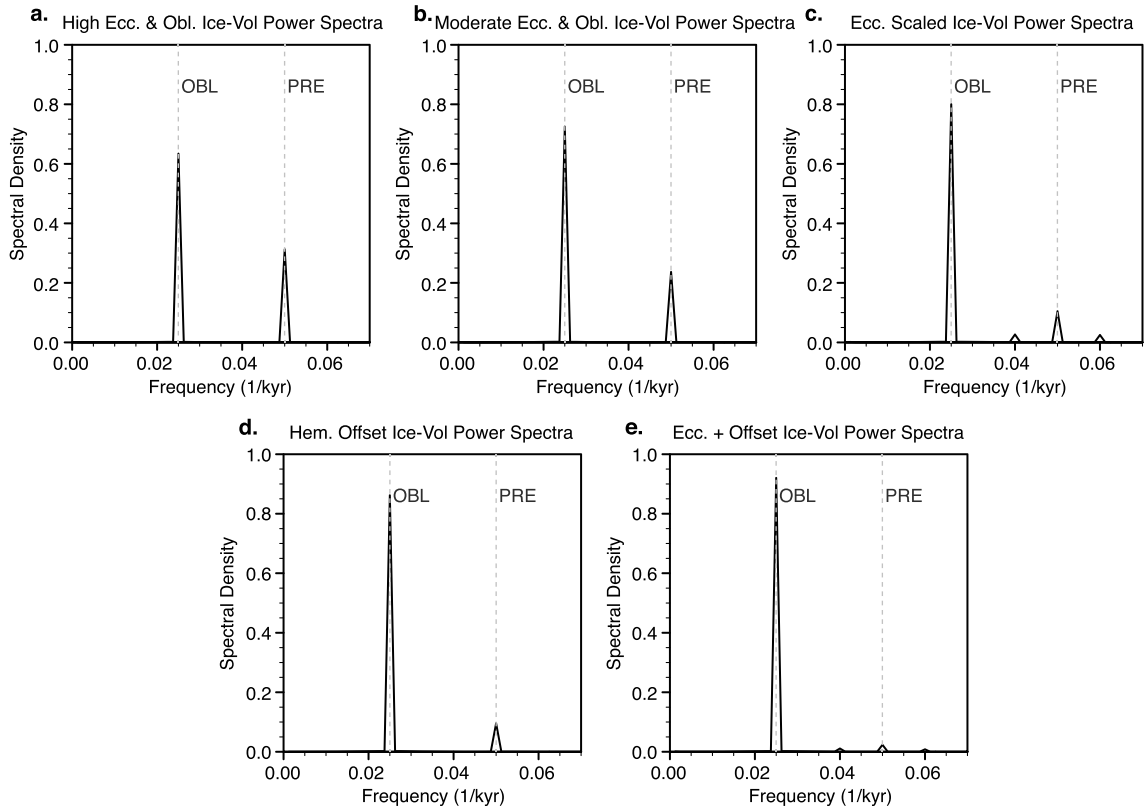

Figure 3. Comparison of standardized ice-volume power spectra responses under different orbital and ice scenarios. (a) Ice-volume spectral power distribution from the high eccentricity and obliquity orbital configuration (OC1). (b) Ice-volume spectral power distribution from the moderate eccentricity and obliquity orbital configuration. A moderate orbit results in a weaker precession ice-volume signal, but the precession signal is still larger than the $\delta^{18}O$ records of the EP. (c) Ice-volume spectral power distribution that includes transient eccentricity modulation of the precession response shows a reduction in the precession power. (d) Ice-volume spectral power distribution of the global ice-volume response that includes contributions from both hemispheres. The precession power is significantly reduced with only 15 m of MSLE fluctuations from Antarctica. (e) The combination of transient eccentricity modulation and ice-volume fluctuations from Antarctica almost completely removes the precession signal, creating the 41 kyr world.

We approximate relative magnitudes of A_o and A_p in our simulations to be 40% and 58% by calculating the HL NA land potential ablation (based on equation (S1)) contributions from obliquity and precession. Due to its lower frequency, we estimate that obliquity accounts for over 58% of the ice-volume signal. The actual ice-volume responses to obliquity and precession are quite similar to this estimate (Figure 1b).

4. Discussion

4.1. Orbital Bias

One cause for the overly large precession ice-volume signal in our model results is our choice of orbital configuration. In these experiments, the value of eccentricity is a larger deviation from the mean orbit (66% difference) than the cycle of obliquity (47% difference). To address this bias, we ran an additional experiment using the OC1 phasing of obliquity and precession with the Pleistocene average eccentricity (0.0285) and obliquity range (22.791–24.085). The total ice-volume response decreases with a more moderate transient orbit (22 m versus 31 m), and the resulting ice-volume spectral power distribution transfers signal strength to the obliquity frequency (73%) compared to the default OC1 configuration (63%) (Figure 3b). Nonetheless, the precession ice-volume signal strength remains larger than that observed in $\delta^{18}O$ records of the EP [*Lisiecki and Raymo*, 2005; *Huybers*, 2007].

An additional bias in our orbital configuration is that eccentricity remains constant, giving precession a large insolation forcing every 20 kyr instead of every 100 kyr or 400 kyr. We approximate the effect of transient eccentricity on modeled ice-volume spectral power distribution by decomposing the ice-volume signals into obliquity and precession components, then temporally scaling the precession signal amplitude by the percent

difference between the original eccentricity (0.056596) and a 100 kyr eccentricity cycle (0.000267–0.056596). Recombining the obliquity ice-volume component with the scaled precession ice-volume component produces an eccentricity cycle-modulated ice-volume signal. The resulting spectral power distribution amplifies the obliquity power from 63% to 80% and reduces the precession power to 10% (Figure 3c).

4.2. Ice-Volume Hemispheric Offset

Another consideration is that the δ^{18}O ice-volume record is not completely driven by NH forcing [*Raymo et al*., 2006]. Because insolation forcing from precession is out of phase between hemispheres and ocean δ^{18}O proxies record global ice-volume, precession might have a significant influence on local ice-volume without producing a global δ^{18}O signal. *Raymo et al*. [2006] show that changes in Antarctic ice-volume during the EP can cause the precession signal to vanish from the δ^{18}O records. Given the already relatively small precession ice-volume signal strength in our model results, the precession signal also disappears with minimal variations in Southern Hemisphere (SH) ice-volume. If we assume that other EP ice sheets, including the Fennoscandian and Antarctic ice sheets, respond to orbital forcing in a similar manner to our NA ice sheets, we can scale our ice-volume signal to match the estimated EP MSLE variability of ~70 m [*Sosdian and Rosenthal*, 2009]. As an example, if we use the ice-volume signal from OC1 to represent the NH ice-volume response and assume SH variations equivalent to 15 m MSLE in combination with ice δ^{18}O compositions of -30‰ and -45‰ for NH and SH ice, respectively [*Raymo et al*., 2006], the precession signal contribution to the global δ^{18}O signal reduces to less than 10% with only 15 m of MSLE contribution from Antarctica (Figure 3d). Further, combining hemispheric offset with eccentricity modulation of the precession signal almost completely removes power at the frequency of precession (2%) (Figure 3e). Note, here we posit that the Antarctic ice sheets respond to orbital forcing in the same manner as the modeled NA ice sheets; however, Antarctica response to orbital forcing is uncertain and might be more significantly influenced by changes in ocean currents than land-based ablation [e.g., *Pollard and DeConto*, 2009]. Nevertheless, our results lend credibility to the hemispheric offset hypothesis given the relatively small amount of Antarctic ice melt required to remove most of the precession signal. Antarctic ice-volume variability of 15 m is reasonable since proxy evidence suggests an unstable East Antarctic Ice Sheet during the late Pliocene, with sea level fluctuations of up to 10 m [*Cook et al*., 2013].

4.3. GHG Fluctuations

Due to the lack of high-resolution atmospheric composition data available for the EP, we omit GHG fluctuations from our experiments. However, other modeling studies suggest a significant role for CO_2 during the last deglaciation [*Abe-Ouchi et al*., 2007]. Further, *Ruddiman* [2003, 2006] shows that during the late Pleistocene CO_2 fluctuations were significantly larger at the frequency of obliquity than precession, and these 41 kyr fluctuations in CO_2 acted nearly in phase with ice-volume, implying a positive feedback. If such a relationship existed during the EP, it would be yet another mechanism to enhance the 41 kyr ice-volume signal. Variations in CO_2 could further reduce the amount of hemispheric offset required to produce the EP δ^{18}O records. However, additional proxy and modeling data are required to discern the magnitude and time of EP CO_2 variability.

4.4. Response Changes After the Mid-Pleistocene Transition

Our simulations address the ice-volume record prior to the mid-Pleistocene transition (MPT), at which point ice-volume varies predominantly at a period of 100 kyr. The change in the response to orbital forcing might be related to ice sheet extent. Summer insolation forcing from obliquity is strongest over the high latitudes and reverses sign below ~45° latitude, while summer insolation forcing from precession remains uniform over much of the hemisphere. Therefore, once an ice sheet reaches lower latitudes, precession controls almost all insolation variability in the main ice sheet ablation zone. The simultaneous appearance of larger NA ice sheets and a stronger eccentricity ice-volume response after the MPT might be a consequence of more extensive ice sheets requiring a greater magnitude, low-latitude forcing to retreat. Furthermore, a more extensive ice sheet would likely not be as susceptible to vegetation feedbacks, further reducing the influence of obliquity. This theory is somewhat dependent on an increasing areal extent of the ice sheets after the MPT. While some research proposes little change in the maximum ice sheet extent through the Pleistocene [e.g., *Clark and Pollard*, 1998], other proxies support a less extensive ice sheet during much of the EP [e.g., *Balco and Rovey*, 2010].

5. Conclusion

Our results illustrate that no single factor completely explains the modeled ice-volume signal. Instead, amplification of the obliquity forcing by sea ice, vegetation, and cloud feedbacks; seasonal offset of the precession forcing; and differences in cycle duration are necessary to understand the contributions of obliquity and precession to ice-volume response. These factors cause obliquity to have the dominate influence on ice sheet variability, in agreement with the Pleistocene $\delta^{18}O$ records [*Lisiecki and Raymo*, 2005; *Huybers*, 2007]. Furthermore, by including eccentricity modulation of the precession ice-volume signal and invoking a reasonably small amount of ice response from Antarctica, we are able to reduce the global ice-volume response to precession and produce a signal that compares favorably with the ice-volume proxy records of the EP. Based on these results, a possible hypothesis for the "41 kyr world" involves a marginally unstable Antarctic ice sheet during the EP, which dampens the precession contribution to the $\delta^{18}O$ records, while albedo feedback amplifications allow obliquity to produce a strong signal throughout the Pleistocene.

Acknowledgments
We are grateful to William Ruddiman and anonymous reviewers whose comments improved this manuscript. We thank the Climate Change Research Laboratory at the University of Michigan for their discussion and suggestions. This research was funded by NSF grant OCE-0902258 awarded to C. Poulsen. Model data are available upon request.

The Editor thanks William Ruddiman and an anonymous reviewer for their assistance in evaluating this paper.

References

Abe-Ouchi, A., T. Segawa, and F. Saito (2007), Climatic Conditions for modelling the Northern Hemisphere ice sheets throughout the ice age cycle, *Clim. Past*, *3*, 423–438, doi:10.5194/cp-3-423-2007.

Alder, J. R., S. W. Hostetler, D. Pollard, and A. Schmittner (2011), Evaluation of a present-day climate simulation with a new coupled atmosphere-ocean model GENMOM, *Geosci. Model Dev.*, *4*, 69–83, doi:10.5194/gmd-4-69-2011.

Balco, G., and C. W. Rovey (2010), Absolute chronology for major Pleistocene advances of the Laurentide Ice Sheet, *Geology*, *38*(9), 795–798, doi:10.1130/G30946.1.

Bender, M. L. (2002), Orbital tuning chronology for the Vostok climate record supported by trapped gas composition, *Earth Planet. Sci. Lett.*, *204*(1–2), 275–289, doi:10.1016/S0012-821X(02)00980-9.

Berger, A., and M. F. Loutre (1991), Insolation values for the climate of the last 10 million years, *Quat. Sci. Rev.*, *10*(4), 297–317, doi:10.1016/0277-3791(91)90033-Q.

Berger, A., X. S. Li, and M. F. Loutre (1999), Modelling northern hemisphere ice volume over the last 3 Ma, *Quat. Sci. Rev.*, *18*(1), 1–11, doi:10.1016/S0277-3791(98)00033-X.

Birchfield, G. E., J. Weertman, and A. T. Lunde (1981), A paleoclimate model of Northern Hemisphere ice sheets, *Quat. Res.*, *15*(2), 126–142, doi:10.1016/0033-5894(81)90100-9.

Clark, P. U., and D. Pollard (1998), Origin of the middle Pleistocene transition by ice sheet erosion of regolith, *Paleoceanography*, *13*(1), 1–9, doi:10.1029/97PA02660.

Claussen, M., J. Fohlmeister, and A. Ganopolski (2006), Vegetation dynamics amplifies precessional forcing, *Geophys. Res. Lett.*, *33*, L00709, doi:10.1029/2006GL026111.

Cook, C. P., et al. (2013), Dynamic behaviour of the East Antarctic Ice Sheet during Pliocene warmth, *Nat. Geosci.*, *6*(9), 765–769, doi:10.1038/NGEO1889.

DeConto, R. M., D. Pollard, P. A. Wilson, H. Palike, C. H. Lear, and M. Pagani (2008), Thresholds for Cenozoic bipolar glaciation, *Nature*, *455*, 652–656, doi:10.1038/nature07337.

Erb, M. P., A. J. Broccoli, and A. C. Clement (2013), The contribution of radiative feedbacks to orbitally driven climate change, *J. Clim.*, *26*(16), 5897–5914, doi:10.1175/JCLI-D-12-00419.1.

Gallimore, R. G., and J. E. Kutzbach (1995), Snow cover and sea-ice sensitivity to generic changes in Earth orbital parameters, *J. Geophys. Res.*, *100*(D1), 1103–1120, doi:10.1029/94JD02686.

Gallimore, R. G., and J. E. Kutzbach (1996), Role of orbitally induced changes in tundra area in the onset of glaciation, *Nature*, *381*(6582), 503–505, doi:10.1038/381503a0.

Herrington, A. R., and C. J. Poulsen (2012), Terminating the last interglacial: The role of ice sheet–climate feedbacks in a GCM asynchronously coupled to an ice sheet model, *J. Clim.*, *25*(6), 1871–1882, doi:10.1175/JCLI-D-11-00218.1.

Horton, D. E., C. J. Poulsen, and D. Pollard (2010), Influence of high-latitude vegetation feedbacks on late Palaeozoic glacial cycles, *Nat. Geosci.*, *3*(8), 572–577, doi:10.1038/ngeo922.

Huybers, P. (2006), Early Pleistocene glacial cycles and the integrated summer insolation forcing, *Science*, *303*(5786), 508–511, doi:10.1126/science.1125249.

Huybers, P. (2007), Glacial variability over the last two million years: An extended depth-derived age model, continuous obliquity pacing, and the Pleistocene progression, *Quat. Sci. Rev.*, *26*(1–2), 37–55, doi:10.1016/j.quascirev.2006.07.013.

Huybers, P., and C. Wunsch (2005), Obliquity pacing of the late Pleistocene glacial terminations, *Nature*, *434*(7032), 491–494, doi:10.1038/nature03401.

Huybers, P., and E. Tziperman (2008), Integrated summer insolation forcing and 40,000-year glacial cycles: The perspective from an ice-sheet/energy-balance model, *Paleoceanography*, *23*, PA1208, doi:10.1029/2007PA001463.

Jackson, C. S., and A. J. Broccoli (2003), Orbital forcing of Arctic climate: Mechanisms of climate response and implications for continental glaciation, *Clim. Dyn.*, *21*(7–8), 539–557, doi:10.1007/s00382-003-0351-3.

Kaplan, J. O., et al. (2003), Climate change and Arctic ecosystems: 2. Modeling, paleodata-model comparisons, and future projections, *J. Geophys. Res.*, *108*(D19), 8171, doi:10.1029/2002JD002559.

Lee, S. Y., and C. J. Poulsen (2005), Tropical Pacific climate response to obliquity forcing in the Pleistocene, *Paleoceanography*, *20*, PA4010, doi:10.1029/2005PA001161.

Lee, S. Y., and C. J. Poulsen (2008), Amplification of obliquity forcing through mean-annual and seasonal atmospheric feedbacks, *Clim. Past*, *4*, 205–213, doi:10.5194/cp-4-205-2008.

Lisiecki, L. E., and M. E. Raymo (2005), A Pliocene-Pleistocene stack of 57 globally distributed benthic $\delta^{18}O$ records, *Paleoceanography*, *20*, PA1003, doi:10.1029/2004PA001071.

Lisiecki, L. E., and M. E. Raymo (2007), Plio–Pleistocene climate evolution: Trends and transitions in glacial cycle dynamics, *Quat. Sci. Rev.*, *26*(1–2), 56–69, doi:10.1016/j.quascirev.2006.09.005.

Loutre, M. F., D. Paillard, F. Vimeux, and E. Cortijo (2004), Does mean annual insolation have the potential to change the climate?, *Earth Planet. Sci. Lett.*, *221*(1–4), 1–14, doi:10.1016/S0012-821X(04)00108-6.

Mantsis, D. F., A. C. Clement, A. J. Broccoli, and M. P. Erb (2011), Climate feedbacks in response to changes in obliquity, *J. Clim.*, *24*(11), 2830–2845, doi:10.1175/2010JCLI3986.1.

Milankovitch, M. (1941), *Kanon der Erdbestrahlung und Seine Andwendung auf das Eiszeiten-Problem*, R. Serbian Acad., Belgrade, Serbia.

Petit, J. R., et al. (1999), Climate and atmospheric history of the past 420,000 years from the Vostok ice core, Antarctica, *Nature*, *399*, 429–436, doi:10.1038/20859.

Philander, S. G., and A. V. Fedorov (2003), Role of tropics in changing the response to Milankovich forcing some three million years ago, *Paleoceanography*, *18*(2), 1045, doi:10.1029/2002PA000837.

Pollard, D. (1980), A simple parameterization for ice sheet ablation rate, *Tellus*, *32*(4), 384–388, doi:10.1111/j.2153-3490.1980.tb00965.x.

Pollard, D., and R. M. DeConto (2009), Modelling West Antarctic ice sheet growth and collapse through the past five million years, *Nature*, *458*, 329–332, doi:10.1038/nature07809.

Pollard, D., and R. M. DeConto (2012), Description of a hybrid ice sheet-shelf model, and application to Antarctica, *Geosci. Model Dev.*, *5*(5), 1273–1295, doi:10.5194/gmd-5-1273-2012.

Ravelo, A. C., D. H. Andreasen, M. Lyle, A. O. Lyle, and M. W. Wara (2004), Regional climate shifts caused by gradual global cooling in the Pliocene epoch, *Nature*, *429*, 263–267, doi:10.1038/nature02567.

Raymo, M. E., and K. Nisancioglu (2003), The 41 kyr world: Milankovitch's other unsolved mystery, *Paleoceanography*, *18*(1), 1011, doi:10.1029/2002PA000791.

Raymo, M. E., L. E. Lisiecki, and K. H. Nisancioglu (2006), Plio-Pleistocene ice volume, Antarctic climate, and the global $\delta^{18}O$ record, *Science*, *313*, 492–495, doi:10.1126/science.1123296.

Robinson, A., R. Calov, and A. Ganopolski (2010), An efficient regional energy-moisture balance model for simulation of the Greenland Ice Sheet response to climate change, *Cryosphere*, *4*(2), 129–144, doi:10.5194/tc-4-129-2010.

Roe, G. (2006), In defense of Milankovitch, *Geophys. Res. Lett.*, *33*, L24703, doi:10.1029/2006GL027817.

Ruddiman, W. F. (2003), Orbital insolation, ice volume, and greenhouse gases, *Quat. Sci. Rev.*, *22*, 1597–1629, doi:10.1016/S0277-3791(03)00087-8.

Ruddiman, W. F. (2006), Orbital changes and climate, *Quat. Sci. Rev.*, *25*, 3092–3112, doi:10.1016/j.quascirev.2006.09.001.

Sosdian, S., and Y. Rosenthal (2009), Deep-sea temperature and ice volume changes across the Pliocene-Pleistocene climate transitions, *Science*, *325*, 306–310, doi:10.1126/science.1169938.

Tabor, C. R., C. J. Poulsen, and D. Pollard (2014), Mending Milankovitch's theory: Obliquity amplification by surface feedbacks, *Clim. Past*, *10*(1), 41–50, doi:10.5194/cp-10-41-2014.

Tuenter, E., S. L. Weber, F. J. Hilgen, L. J. Lourens, and A. Ganopolski (2004), Simulation of climate phase lags in response to precession and obliquity forcing and the role of vegetation, *Clim. Dyn.*, *24*(2–3), 279–295, doi:10.1007/s00382-004-0490-1.

Tuenter, E., S. L. Weber, F. J. Hilgen, and L. J. Lourens (2005), Sea-ice feedbacks on the climatic response to precession and obliquity forcing, *Geophys. Res. Lett.*, *32*, L24704, doi:10.1029/2005GL024122.

van den Berg, J., R. van de Wal, and H. Oerlemans (2008), A mass balance model for the Eurasian ice sheet for the last 120,000 years, *Global Planet. Change*, *61*(3–4), 194–208, doi:10.1016/j.gloplacha.2007.08.015.

Vettoretti, G., and W. R. Peltier (2004), Sensitivity of glacial inception to orbital and greenhouse gas climate forcing, *Quat. Sci. Rev.*, *23*(3–4), 499–519, doi:10.1016/j.quascirev.2003.08.008.